Atomic-coherence-assisted multipartite entanglement generation with dressing-energy-level-cascaded four-wave mixing

Yuliang Liu,* Jiajia Wei,* Mengqi Niu, Yixin Lin, Zhili Chen, Jin Yan, Binshuo Luo, Feng Li, Yin Cai,† and Yanpeng Zhang‡

Key Laboratory for Physical Electronics and Devices of the Ministry of Education, Shaanxi Key Lab of Information Photonic Technique, School of Electronic Science and Engineering, Xi'an Jiaotong University, Xi'an, Shaanxi 710049, China

(Received 22 March 2022; accepted 26 September 2022; published 13 October 2022)

Multipartite entanglement plays an important role in quantum information processing and quantum metrology. Here, the dressing-energy-level-cascaded four-wave mixing (FWM) processes are proposed to generate all-optical controlled multipartite entanglement within a single device. The entanglement characteristics of the produced states of light are characterized by applying the Duan criterion and the positivity under partial transposition criterion. Moreover, by using an internal dressing field to modulate atomic coherence, multiple quantum coherent channels of FWM are simultaneously constructed, which result in a great extension of entanglement mode number and quantum information capacity. We find that the violation of the entanglement criteria inequalities is coherent-channel dependent, and the produced states can be directly modulated via atomic coherence. Our system can integrate the generation and modulation of the entangled states in one process. It may help provide a compact method for realizing large-scale quantum networks.

DOI: 10.1103/PhysRevA.106.043709

I. INTRODUCTION

Multipartite entanglement has garnered a lot of attention because of its significance and potential applications in quantum information processing and quantum metrology [1–5]. A mature technology for generating multiphoton entangled states is applying multiple spontaneous parametric down-conversion processes, which produce down-converted photon pairs in a second-order nonlinear crystal [6–10]. Continuous-variable multipartite entanglement can be implemented by using multiple optical parametric oscillators [11–17]. Additionally, many alternative methods to produce multipartite entanglement have been demonstrated, such as quantum frequency combs [18,19], spatial modes [20], and temporal entanglement [21,22]. Hitherto, multipartite entanglement has been widely applied in quantum sensing [23–25], quantum computing [26–28], and constructing quantum networks [29,30].

In recent years, another effective method for preparing entanglement is using the four-wave mixing (FWM) process of atomic media. Entangled light beams have been experimentally verified through a parametric amplified (PA) FWM process in high-gain atomic media [30–33]. The FWM process exhibits unique advantages. It has the nature of a spatial multimode, and the produced entangled light beams are spatially separated [34,35]. Also, due to the strong nonlinearity, the optical cavity is not required, and therefore, the experimental setup is simplified. With the features of scalability and flexibility, many methods to prepare multipartite entanglement using FWM have been theoretically proposed and experimentally demonstrated, including a multipump [36,37] and cascading atomic cells [38–41]. However, the effect of the atomic coherence, which is important for generating and modulating multipartite entanglement in atomic ensemble, has not been explored.

In an atomic ensemble, the nonlinear susceptibility of FWM can be actively modulated based on atomic coherence. The induced dressing effect can be used to reshape the parametric gain profile of FWM and realize coherent control of the quantum entanglement. Moreover, via splitting atomic energy levels with the dressing effect, the frequency modes of the correlated photons can be extended to construct multiple coherent channels of FWM, and it results in hyperentanglement and energy-time entanglement [42–44]. Also, with the constructive interference among different transition probability amplitudes, the conversion efficiency of the FWM process may increase, and therefore, the degree of squeezing states of light can be enhanced by modulating the internal states of a multilevel atomic system [45–47].

In this paper, multipartite entangled states of light are produced from dressing-energy-level-cascaded (DELC) FWM in one step. This scheme employs a single device of hot rubidium atomic medium and exhibits advantages such as simplified experimental devices, lower optical path losses, and fewer vacuum losses. We apply the Duan [48] and the positivity under partial transposition (PPT) [49,50] criteria to investigate the multipartite entanglement of the output beams. Furthermore, we introduce the dressing field to simultaneously construct multiple coherent channels of FWM, thereby realizing multimode entanglement and expanding the quantum information capacity. In this paper, with atomic

*These authors contributed equally to this work.
†caiyin@mail.xjtu.edu.cn
‡ypzhang@mail.xjtu.edu.cn

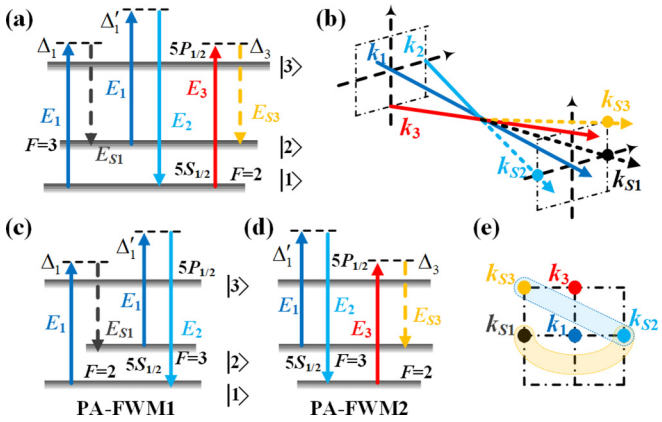

FIG. 1. (a) Energy-level diagram of the three-mode dressing-energy-level-cascaded (DELC)-four-wave mixing (FWM) processes in the rubidium atomic system. (b) The spatial distribution of the beams. The arrows represent the signal beams. The angles are determined by the phase-matching conditions, and the intersection point is the Rb cell. $\mathbf{k}_i$ is the wave vector of $\mathbf{E}_i$ ($i = 1, 2, 3, S1, S2, S3$). (c) Energy-level diagram of parametric amplified (PA)-FWM1 process. (d) Energy-level diagram of PA-FWM2 process. (e) The tangential distribution of output signal beams. The belts indicate quantum correlation existing between the two connected modes.

coherence, the generation and modulation of multipartite entanglement can be integrated in the process of the entangled state preparation. These results may be helpful for providing a compact way in multimode quantum secure communication, quantum computing, and quantum sensing.

II. THEORETICAL MODEL OF DELC-FWM PROCESSES

A. Generation of three-mode outputs

We consider a double-Λ-type three-level $|1\rangle$-$|2\rangle$-$|3\rangle$ atomic system, as shown in Fig. 1. One possible experimental candidate for the proposed system is $5S_{1/2}, F = 2(|1\rangle)$, $5S_{1/2}$, $F = 3$ $(|2\rangle)$ and $5P_{1/2}$, $(|3\rangle)$ in ^{85}Rb. The atom is driven from $|1\rangle$ to $|3\rangle$ (with an energy mismatch) with a beam of energy $\mathbf{E}_1$ (frequency ω_1, wave vector $\mathbf{k}_1$, and Rabi frequency Ω_1), from where it decays to $|2\rangle$, emitting a photon in mode $\mathbf{E}_{S1}$. It is then again excited by the same driving beam, from where it can decay to the ground state, emitting a photon with energy $\mathbf{E}_2$ (ω_2, $\mathbf{k}_2$, and Ω_2), $\mathbf{E}_2 = \mathbf{E}(|3\rangle) - \boldsymbol{E}(|1\rangle) + \Delta_1^{'}$. The atom is driven from $|1\rangle$ to $|3\rangle$ (with an energy mismatch) with a beam of energy $\mathbf{E}_3$ (ω_3, $\mathbf{k}_3$, and Ω_3), from where it decays to $|2\rangle$, emitting a photon with energy E_{S3}, $\mathbf{E}_{S3} = \mathbf{E}(|3\rangle) - \mathbf{E}(|2\rangle) + \Delta_3$.

The entire process can be viewed as two PA-FWM processes [Figs. 1(c) and 1(d)] cascaded together, which corresponds to two cascading Rb cells, as shown in Fig. 2. The detuning Δ_i is defined as the difference between the resonant transition frequency and the laser frequency of $\mathbf{E}_i$. With the detuning of $\mathbf{E}_1$ tuned far away from the resonance, PA-FWM1 and PA-FWM2 will occur in the system, which can generate the quantum correlated output beams $\mathbf{E}_{S1}$, $\mathbf{E}_{S2}$ (amplified $\mathbf{E}_2$), and $\mathbf{E}_{S3}$ in a single Rb cell satisfying the phase-match conditions $\mathbf{k}_{S1} + \mathbf{k}_{S2} = 2\mathbf{k}_1$ and $\mathbf{k}_{S2} + \mathbf{k}_{S3} = \mathbf{k}_1 + \mathbf{k}_3$, respectively.

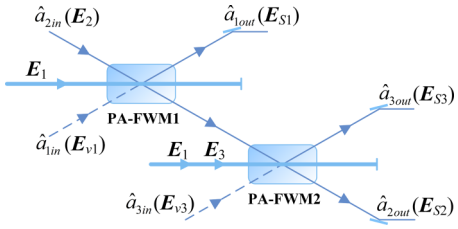

FIG. 2. Schematic diagram of cascading two Rb cells to generate three-mode entangled states. $\hat{a}_{2in}$ is the seed input signal; $\hat{a}_{1in}$ and $\hat{a}_{3in}$ are the vacuum input signals. $\mathbf{E}_2$ is amplified by PA-FWM1 and injected into PA-FWM2. $\hat{a}_{1\text{out}}$, $\hat{a}_{2\text{out}}$, and $\hat{a}_{3\text{out}}$ are three output signals.

In this DELC-FWM system, three inputs $\mathbf{E}_1$, $\mathbf{E}_2$, and $\mathbf{E}_3$ converge in the Rb cell and generate three spatially separated outputs $\mathbf{E}_{S1}$, $\mathbf{E}_{S2}$ (amplified $\mathbf{E}_2$), and $\mathbf{E}_{S3}$ by cascading two PA-FWM processes. Here, PA-FWM1 and PA-FWM2 processes can be symbolized in simple terms by a phenomenological Hamiltonian as follows [51]:

$$H_1 = i\hbar\kappa_1'\hat{b}_1\hat{a}_1^\dagger\hat{b}_1\hat{a}_2^\dagger + \text{H.c.}, \tag{1a}$$

$$H_2 = i\hbar\kappa_2'\hat{b}_2\hat{a}_2^\dagger\hat{b}_2\hat{a}_3^\dagger + \text{H.c.}, \tag{1b}$$

where κ_1' and κ_2' describe the strength of the nonlinear interaction. Here, $\hat{a}_1^\dagger$, $\hat{a}_2^\dagger$, and $\hat{a}_3^\dagger$ are the boson operators for the output modes of $\mathbf{E}_{S1}$, $\mathbf{E}_{S2}$, and $\mathbf{E}_{S3}$, respectively; $\hat{b}_1$ and $\hat{b}_2$ are the boson operators for the pump fields $\mathbf{E}_1$ and $\mathbf{E}_3$, respectively. Also, H.c. is Hermitian conjugate. The provided pump fields are of sufficient intensity that they may be treated classically and as nondepleting. Therefore, Eqs. (1a) and (1b) can be rewritten as

$$H_1 = i\hbar\kappa_1\hat{a}_1^\dagger\hat{a}_2^\dagger + \text{H.c.}, \tag{2a}$$

$$H_2 = i\hbar\kappa_2\hat{a}_2^\dagger\hat{a}_3^\dagger + \text{H.c.}, \tag{2b}$$

where $\kappa_1 = -i\varpi_1\chi_1^{(3)}E_1^2/2c$ and $\kappa_2 = -i\varpi_2\chi_2^{(3)}E_1E_3/2c$; κ_1 and κ_2 physically depend on the central frequency of generated signals ϖ_i, the third-order nonlinear susceptibility $\chi_1^{(3)}$ and $\chi_2^{(3)}$, and the intensity of the pump field, and practically depend on the atomic temperature (i.e., atomic density), phase-matching angle of the fields, etc.

The boson-creation (annihilation) operator satisfies the Heisenberg operator of motion in the dipole approximation. The dynamic equation of the system can be written as $\frac{d\hat{a}_i}{dt} = \frac{-i}{\hbar}[\hat{a}_i, H]$, $(i = 1, 2, 3)$, from which we obtain

$$\text{PA-FWM1}: \frac{d\hat{a}_1}{dt} = \kappa_1\hat{a}_2^\dagger, \quad \frac{d\hat{a}_2}{dt} = \kappa_1\hat{a}_1^\dagger, \tag{3a}$$

$$\text{PA-FWM2}: \frac{d\hat{a}_2}{dt} = \kappa_2\hat{a}_3^\dagger, \quad \frac{d\hat{a}_3}{dt} = \kappa_2\hat{a}_2^\dagger. \tag{3b}$$

After the operation of time evolution equation, the final input-output relations of this system are

$$\hat{a}_{1\text{out}} = G_1\hat{a}_{1\text{in}} + g_1\hat{a}_{2\text{in}}^\dagger, \tag{4a}$$

$$\hat{a}_{2\text{out}} = g_1G_2\hat{a}_{1\text{in}}^\dagger + G_1G_2\hat{a}_{2\text{in}} + g_2\hat{a}_{3\text{in}}^\dagger, \tag{4b}$$

$$\hat{a}_{3\text{out}} = g_1g_2\hat{a}_{1\text{in}} + G_1g_2\hat{a}_{2\text{in}}^\dagger + G_2\hat{a}_{3\text{in}}, \tag{4c}$$

where $G_1 = \cosh(\kappa_1 t)$ and $G_2 = \cosh(\kappa_2 t)$ are the amplitude gain in PA-FWM1 and PA-FWM2, respectively; $G_i^2 - g_i^2 = 1$ $(i = 1, 2)$. Here, t is the interaction time which can be adjusted by changing the length and temperature of the Rb vapor in experiment. Also, $\hat{a}_{1\text{in}}^\dagger$, $\hat{a}_{2\text{in}}^\dagger$, and $\hat{a}_{3\text{in}}^\dagger$ ($\hat{a}_{1\text{in}}$, $\hat{a}_{2\text{in}}$, and $\hat{a}_{3\text{in}}$) are the creation (annihilation) operators of inputs $\mathbf{E}_1$, $\mathbf{E}_2$, and $\mathbf{E}_3$, respectively; and $\hat{a}_{1\text{out}}$, $\hat{a}_{2\text{out}}$, and $\hat{a}_{3\text{out}}$ are the annihilation operators of the outputs $\mathbf{E}_{S1}$, $\mathbf{E}_{S2}$, and $\mathbf{E}_{S3}$, respectively. The amplitude and phase quadrature operators are defined as $\hat{X} = \hat{a} + \hat{a}^\dagger$ and $\hat{P} = i(\hat{a}^\dagger - \hat{a})$. A vector of canonical quadrature operators is defined as $\mathbf{r} = (\hat{X}_1, \hat{P}_1, \cdots, \hat{X}_n, \hat{P}_n)$. The evolution equations of the three output modes can be written as $\mathbf{r}_{\text{out}} = \mathbf{U}_{\text{tri}}\mathbf{r}_{\text{in}}$, where the transform operation matrix $\mathbf{U}_{\text{tri}}$ is

$$\mathbf{U}_{\text{tri}} = \begin{pmatrix} G_1 & 0 & g_1 & 0 & 0 & 0 \\ 0 & G_1 & 0 & -g_1 & 0 & 0 \\ g_1 G_2 & 0 & G_1 G_2 & 0 & g_2 & 0 \\ 0 & -g_1 G_2 & 0 & G_1 G_2 & 0 & -g_2 \\ g_1 g_2 & 0 & G_1 g_2 & 0 & G_2 & 0 \\ 0 & g_1 g_2 & 0 & -G_1 g_2 & 0 & G_2 \end{pmatrix}. \tag{5}$$

The quantum correlations of multimode Gaussian states generated by a quadratic Hamiltonian can be fully characterized by its covariance matrix (CM). The elements of the CM are defined as follows:

$$\sigma_{ij} = \tfrac{1}{2}\langle \hat{r}_i \hat{r}_j + \hat{r}_j \hat{r}_i \rangle - \langle \hat{r}_i \rangle \langle \hat{r}_j \rangle. \tag{6}$$

According to the definition of the CM, we can reconstruct the CM as $\boldsymbol{\sigma} = \mathbf{U}_{\text{tri}}\mathbf{U}_{\text{tri}}^{\text{T}}$ based on Eq. (5) with the inputs of coherent or vacuum states. Note that there does not exist cross-correlation between the amplitude and phase quadrature in this system, and the CM is positive and symmetric.

B. Generation of four-mode outputs

The relevant energy level to generate four-mode Gaussian states in the Rb atomic system is the same as that in the three-mode case, but the pump field $\mathbf{E}_3$ (ω_3, $\mathbf{k}_3$, and Ω_3) drives the transitions $|1\rangle \to |3\rangle$ and $|2\rangle \to |3\rangle$ with frequency detuning Δ_3 and $\Delta_3^{'}$, respectively. This four-mode DELC-FWM system contains an eight-wave mixing process, as shown in Fig. 3, which satisfies the phase-match condition $2\mathbf{k}_1 + 2\mathbf{k}_3 = \mathbf{k}_{S1} + \mathbf{k}_2 + \mathbf{k}_{S3} + \mathbf{k}_{S4}$ and four FWM processes that satisfy $2\mathbf{k}_1 = \mathbf{k}_{S1} + \mathbf{k}_2$, $\mathbf{k}_1 + \mathbf{k}_3 = \mathbf{k}_2 + \mathbf{k}_{S3}$, $\mathbf{k}_1 + \mathbf{k}_3 = \mathbf{k}_{S1} + \mathbf{k}_{S4}$, and $2\mathbf{k}_3 = \mathbf{k}_{S3} + \mathbf{k}_{S4}$, respectively. One of the simplified methods to obtain the input-output relations is to view the system as three PA-FWM processes cascaded, which corresponds to cascading three Rb cells, as shown in Fig. 4 [52]. The outputs of PA-FWM1, amplified $\mathbf{E}_2$ and $\mathbf{E}_{v0}$, are injected into PA-FWM2 and PA-FWM3, respectively. The interaction Hamiltonian of these three PA-FWM processes can be expressed as

$$H_1 = i\hbar\kappa_1 \hat{a}_1^\dagger \hat{a}_2^\dagger + \text{H.c.}, \tag{7a}$$

$$H_2 = i\hbar\kappa_2 \hat{a}_2^\dagger \hat{a}_3^\dagger + \text{H.c.}, \tag{7b}$$

$$H_3 = i\hbar\kappa_3 \hat{a}_1^\dagger \hat{a}_4^\dagger + \text{H.c.} \tag{7c}$$

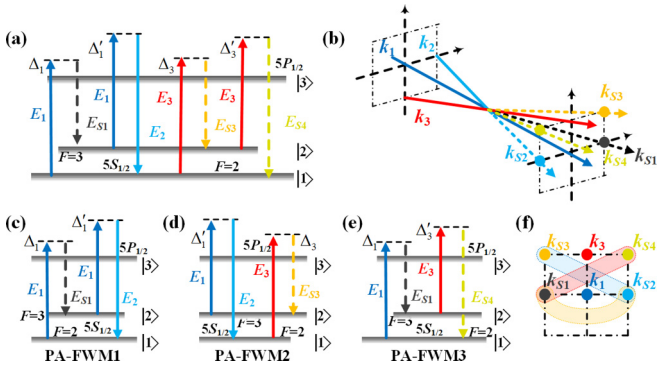

FIG. 3. (a) Energy-level diagram of the four-mode dressing-energy-level-cascaded (DELC)-four-wave mixing (FWM) processes in the rubidium atomic system. (b) The spatial distribution of the beams. The arrows represent the signal beams. The angles are determined by the phase-matching conditions. (c)–(e) Step breakdown energy-level diagram of the subsystem. Three of the four parametric amplified (PA)-FWM processes can compose the four mode DELC-FWM processes. (f) The tangential distribution of output signal beams. The belts indicate quantum correlation existing between the two connected modes.

The amplitude gain and interaction strength are as follows:

$$G_1 = \cosh(\kappa_1 t), \quad \kappa_1 = -\frac{i\varpi_1 \chi_1^{(3)} E_1^2}{2c}, \tag{8a}$$

$$G_2 = \cosh(\kappa_2 t), \quad \kappa_2 = -\frac{i\varpi_2 \chi_2^{(3)} E_1 E_3}{2c}, \tag{8b}$$

$$G_3 = \cosh(\kappa_3 t), \quad \kappa_3 = -\frac{i\varpi_3 \chi_3^{(3)} E_3^2}{2c}. \tag{8c}$$

Using a method like the three-mode system, we can obtain the final input-output relations and then obtain the CM. The transform operation matrix $\mathbf{U}_{\text{quad}}$ in this four-mode system can

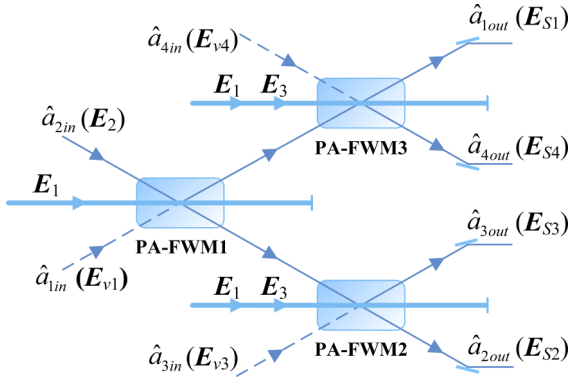

FIG. 4. Schematic diagram of cascading three Rb cells to generate four-mode entangled states. $\hat{a}_{2in}$ is the seed input signal; $\hat{a}_{1in}$, $\hat{a}_{3in}$, and $\hat{a}_{4in}$ are the vacuum input signals. The amplified $\mathbf{E}_2$ and amplified $\mathbf{E}_{v1}$ via the PA-FWM1 process are injected into PA-FWM2 and PA-FWM3, respectively. $\hat{a}_{1\text{out}}$, $\hat{a}_{2\text{out}}$, $\hat{a}_{3\text{out}}$, and $\hat{a}_{4\text{out}}$ are four output signals.

be written as

$$\mathbf{U}_{\text{quad}}=\begin{pmatrix} G_1G_3 & 0 & g_1G_3 & 0 & 0 & 0 & g_3 & 0 \\ 0 & G_1G_3 & 0 & -g_1G_3 & 0 & 0 & 0 & -g_3 \\ g_1G_2 & 0 & G_1G_2 & 0 & g_2 & 0 & 0 & 0 \\ 0 & -g_1G_2 & 0 & G_1G_2 & 0 & -g_2 & 0 & 0 \\ g_1g_2 & 0 & G_1g_2 & 0 & G_2 & 0 & 0 & 0 \\ 0 & g_1g_2 & 0 & -G_1g_2 & 0 & G_2 & 0 & 0 \\ G_1g_3 & 0 & g_1g_3 & 0 & 0 & 0 & G_3 & 0 \\ 0 & -G_1g_3 & 0 & g_1g_3 & 0 & 0 & 0 & G_3 \end{pmatrix}. \tag{9}$$

III. MULTIPARTITE ENTANGLEMENT

In this section, Duan and PPT criteria are used to investigate the multipartite entanglement of the generated quantum Gaussian states. The inequalities of the Duan criterion using the quantum correlations of the associated modes are defined as follows:

$$D_{ij} = V(\hat{X}_i - \hat{X}_j) + V(\hat{Y}_i + \hat{Y}_j) \geqslant 4, \tag{10}$$

where $V(\hat{X}_i - \hat{X}_j)$ is the variance of the difference of the amplitude quadratures, and $V(\hat{Y}_i + \hat{Y}_j)$ is the sum of the phase quadratures. The values D_{ij} suggest the amount of the inseparability. The bipartite entanglement between modes $\hat{a}_i$ and $\hat{a}_j$ can be demonstrated by the violation of the inequalities.

The PPT criterion can be used to characterize the entanglement of two subsystems which consist of one or several modes, and the smaller symplectic eigenvalue suggests the inseparability. It is a sufficient and necessary criterion for the case of 1 vs n modes (1-n) and only sufficient for the case of m-n. For bipartite entanglement of σ_{AB}, the partial transposition operation on part A is equivalent to the transformation through matrix $\mathbf{T}_{\text{A}} = [\oplus_{k=1}^{m}\text{diag}(1,-1)]_{\text{A}} \oplus \mathbf{I}_{\text{B}}$, where the first factor is its mirror reflection in phase space, and the second factor represents the other subsystems. The criterion will lead to the following uncertainty: $\tilde{\sigma}_{\text{AB}} + i\mathbf{\Omega} \geqslant 0$, where $\tilde{\sigma}_{\text{AB}} = \mathbf{T}_{\text{A}}\boldsymbol{\sigma}_{\text{AB}}\mathbf{T}_{\text{A}}$, and $\mathbf{\Omega}$ is the symplectic form with the same dimensions as $\tilde{\sigma}_{\text{AB}}$. The existence of negative symplectic eigenvalues directly means the presence of entanglement.

A. Three-mode outputs

The Duan criterion can be applied to verify any two modes of the three produced modes $\hat{a}_1$, $\hat{a}_2$, and $\hat{a}_3$. In the three-mode system, the values of the Duan criterion D_{12}, D_{13}, and D_{23} are given by

$$D_{12} = 4\left[G_1^2\left(G_2^2+1\right) - 2G_1G_2\sqrt{G_1^2-1} - 1\right], \tag{11a}$$

$$D_{13} = 4G_1^2G_2^2, \tag{11b}$$

$$D_{23} = -4G_1^2\left(2G_2\sqrt{G_2^2-1} - 2G_2^2 + 1\right). \tag{11c}$$

The expressions show the dependence of D_{12}, D_{13}, and D_{23} on the gains G_1 and G_2. The region plots are shown in Fig. 5. The amount of the inseparability $D_{ij} > 4$ means no entanglement. The entanglement regions of modes $\hat{a}_1$ and $\hat{a}_2$ ($D_{12} < 4$) are the blue regions I and III in Fig. 5(a). The entanglement between modes $\hat{a}_1$ and $\hat{a}_2$ is very sensitive to G_2. They entangle when G_2 is smaller because only beam $\hat{a}_2$ is amplified with the second PA-FWM process, which leads to their quantum noise unbalance. Here, $D_{13} > 4$ for any $G_1 > 1$ and $G_2 > 1$ in Fig. 5(c). This is because modes $\hat{a}_1$ and $\hat{a}_3$ do not interact with each other in the Hamiltonian in Eqs. (2a) and (2b), and thus, there is never entanglement existing between modes $\hat{a}_1$ and $\hat{a}_3$. The entanglement regions of modes $\hat{a}_2$ and $\hat{a}_3$ ($D_{23} < 4$) are the orange regions II and III in Fig. 5(a). The entanglement of modes $\hat{a}_2$ and $\hat{a}_3$ is limited by bigger G_1, that is, a bigger G_1 is not helpful in the presence of the entanglement.

The PPT criterion is also verified in this three-mode system as shown in Fig. 6. The PPT criterion can be used to characterize the bipartite and tripartite entanglement. The value of the PPT criterion <0 directly means the presence of entanglement. The results of the bipartite entanglement characterized by the PPT criterion are like the Duan criterion. The PPT value of $\hat{a}_1 - \hat{a}_3 > 0$ for any $G_1 > 1$ and $G_2 > 1$, which is consistent with previous analysis. The entanglement exists in all 1–2 mode types. We find the trends of tripartite entanglement $\hat{a}_1 - \{\hat{a}_2\hat{a}_3\}$ and $\hat{a}_3 - \{\hat{a}_1\hat{a}_2\}$ are like the entanglement of $\hat{a}_1 - \hat{a}_2$ and $\hat{a}_2 - \hat{a}_3$, respectively, i.e., the conjugate beam $\hat{a}_1$

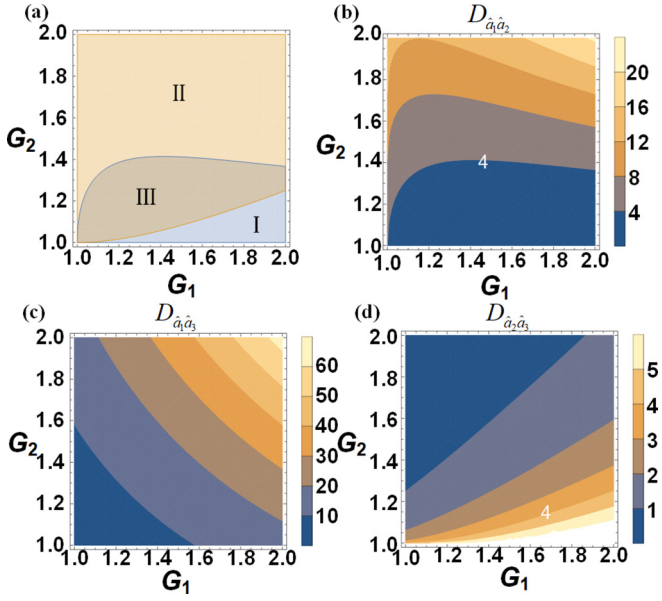

FIG. 5. Bipartite entanglement for the three-mode dressing-energy-level-cascaded (DELC)-four-wave mixing (FWM) processes using the Duan criterion. (a) Only D_{12} is <4 in region I. Only D_{23} is <4 in region II. D_{12} and D_{23} are both <4 in region III. (b)–(d) Duan values of D_{12}, D_{13}, and D_{23} with different values of the gains G_1 and G_2.

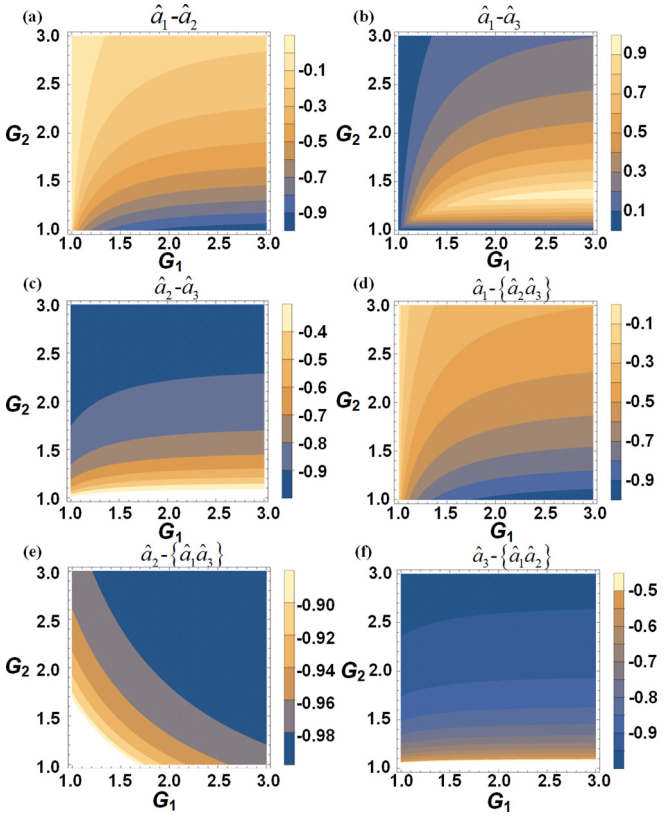

FIG. 6. Positivity under partial transposition (PPT) values of the three-mode dressing-energy-level-cascaded (DELC)-four-wave mixing (FWM) processes. (a)–(c) Bipartite and (d)–(f) tripartite entanglement region plots.

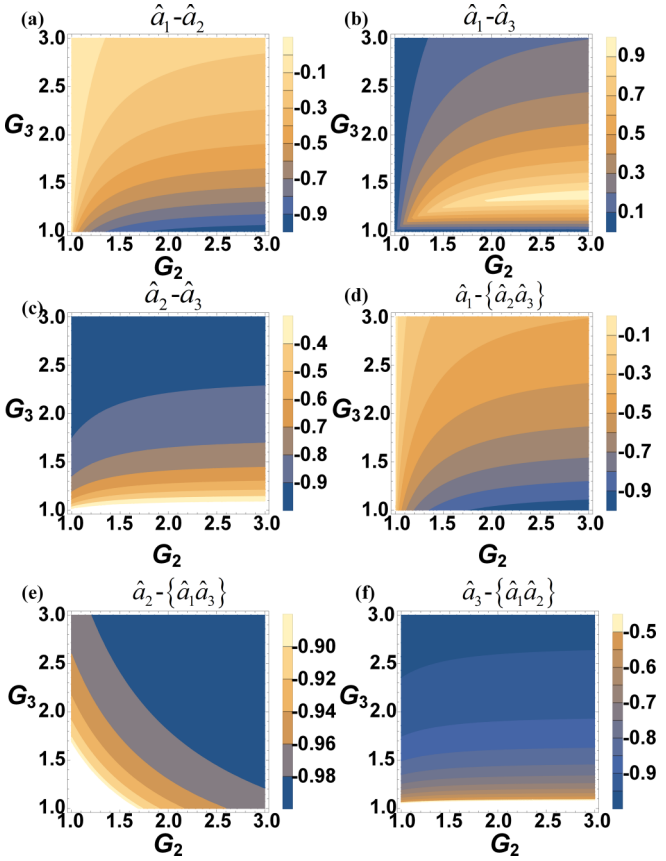

FIG. 7. Bipartite entanglement for the four-mode dressing-energy-level-cascaded (DELC)-four-wave mixing (FWM) processes using the Duan criterion. (a)–(f) Contour plot of D_{12}, D_{13}, D_{14}, D_{23}, D_{24}, and D_{34} with different values of gains G_2 and G_3 at $G_1 = 1.1$.

or $\hat{a}_3$ added with the probe beam $\hat{a}_2$ becoming $\{\hat{a}_1\hat{a}_2\}$ or $\{\hat{a}_2\hat{a}_3\}$ can only quantitatively change the amount of entanglement and does not change the dependence on parameters G_1 and G_2.

B. Four-mode outputs

In the four-mode system, all possible two-mode permutations of the Duan criterion are verified, and the dependence of Duan values on the gains G_1, G_2, and G_3 are shown in Eqs. (12a)–(12e). The corresponding contour plots are shown in Fig. 7, where we set the gain of the first PA-FWM process as 1.1:

$$D_{12} = 4\left(G_1^2G_2^2 + G_1^2G_3^2 - 2G_1G_2G_3\sqrt{G_1^2-1} - 1\right), \quad (12a)$$

$$D_{13} = D_{24} = 4G_1^2\left(G_2^2 + G_3^2 - 1\right), \quad (12b)$$

$$D_{14} = 4G_1^2\left(2G_3^2 - 2G_3\sqrt{G_3^2-1} - 1\right), \quad (12c)$$

$$D_{23} = 4G_1^2\left(2G_2^2 - 2G_2\sqrt{G_2^2-1} - 1\right), \quad (12d)$$

$$D_{34} = 4\begin{pmatrix} -2G_1^2 + G_1^2G_2^2 + G_1^2G_3^2 \\ -2G_1\sqrt{G_1^2-1}\sqrt{G_2^2-1}\sqrt{G_3^2-1} + 1 \end{pmatrix}. \quad (12e)$$

The values of D_{12}, D_{13}, D_{24}, and D_{34} all go up with the increasing G_2 and G_3, suggesting that stronger G_2 and G_3 do not help in enhancing the entanglement for a fixed G_1. Moreover, D_{14} (D_{23}) changes with the gain G_1 and G_3 (G_1 and G_2) because modes $\hat{a}_1$ and $\hat{a}_4$ (modes $\hat{a}_2$ and $\hat{a}_3$) never participate in the PA-FWM2 (PA-FWM3) process, and therefore, gain G_2 (G_3) does not contribute to the entanglement between these two modes.

The dependence of the PPT criterion on gain G_1 in the four-mode system is shown in Fig. 8. Here, we set the values $G_2 = 1.3$ and $G_3 = 1.1$. The PPT values of $\hat{a}_1 - \hat{a}_3$, $\hat{a}_2 - \hat{a}_4$, and $\hat{a}_3 - \hat{a}_4$ are not negative when $G_1 > 1$, meaning the absence of entanglement, which are like the Duan criterion. The modes $\hat{a}_1$ and $\hat{a}_2$ do not entangle when G_1 is small because the interaction of these two modes is not strong enough in the Hamiltonian in Eq. (7a). The entanglement of the three-mode subsystem in the four-mode system is all verified in Figs. 8(b)–8(d). Here, $\hat{a}_3-\{\hat{a}_1\hat{a}_4\}$ and $\hat{a}_4-\{\hat{a}_2\hat{a}_3\}$ do not entangle and therefore are not given in this figure. This is because mode $\hat{a}_3$ ($\hat{a}_4$) does not interact with any one mode of modes $\{\hat{a}_1\hat{a}_4\}$ ($\{\hat{a}_2\hat{a}_3\}$) in this symmetrical structure. The PPT values of 1-3 modes and 2-2 modes are all <0 when $G_1 > 1$. However, increasing G_1 slightly decreases the entanglement of $\{\hat{a}_1\hat{a}_2\} - \{\hat{a}_3\hat{a}_4\}$, $\hat{a}_3-\{\hat{a}_1\hat{a}_2\hat{a}_4\}$, and $\hat{a}_4-\{\hat{a}_1\hat{a}_2\hat{a}_3\}$.

IV. COHERENT CHANNELS WITH DRESSING EFFECT

In this section, we turn our attention to the atomic coherence control. We will start from the Hamiltonian of the

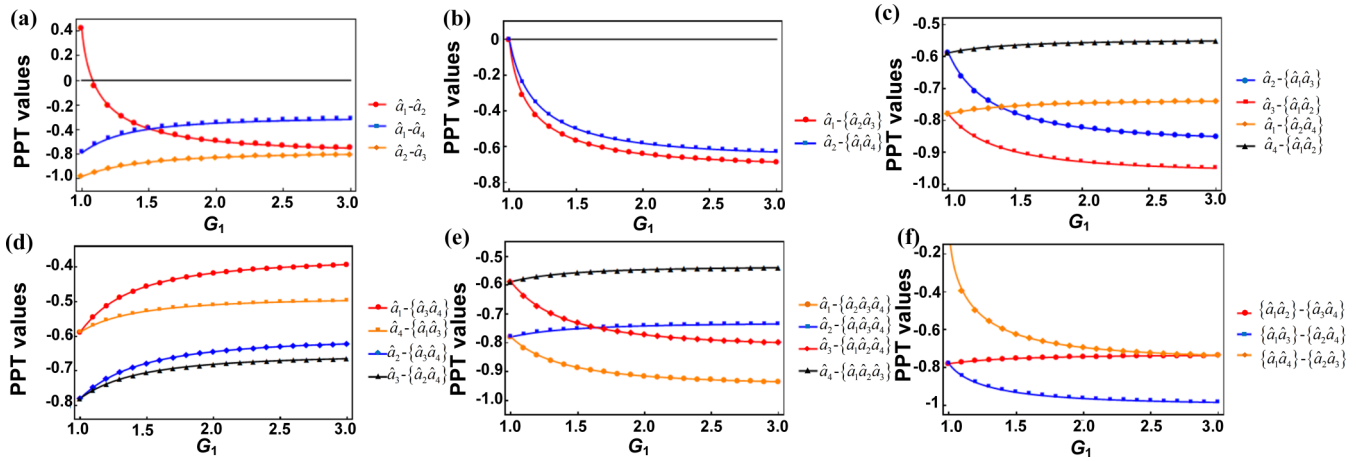

FIG. 8. PPT values of the four-mode DELC-FWM processes with increasing G_1 at $G_2 = 1.3$ and $G_3 = 1.1$. (a) Bipartite entanglement. (b)–(d) Tripartite entanglement. (e) and (f) Quadripartite entanglement (two types of 1-3 and 2-2 modes).

system and finally obtain the third-order density matrix element, which is the microscopic expression of the third-order nonlinear susceptibility.

As an example, the effective Hamiltonian H_{eff} of the PA-FWM1 process is as follows:

$$H_{\text{eff}} = \hbar \begin{pmatrix} 0 & 0 & -\frac{1}{2}\Omega_1^* & -\frac{1}{2}\Omega_{S2}^* \\ 0 & \Delta_1 - \Delta_{S1} - \frac{1}{2}i\Gamma_2 & -\frac{1}{2}\Omega_{S1}^* & -\frac{1}{2}\Omega_1^* \\ -\frac{1}{2}\Omega_1 & -\frac{1}{2}\Omega_{S1} & \Delta_1 - \frac{1}{2}i\Gamma_3 & 0 \\ -\frac{1}{2}\Omega_{S2} & -\frac{1}{2}\Omega_1 & 0 & \Delta_1 - \Delta_{S1} + \Delta'_1 - \frac{1}{2}i\Gamma_4 \end{pmatrix}. \tag{13}$$

According to the Heisenberg-Langevin equation:

$$\frac{\partial}{\partial t}\boldsymbol{\rho} = \frac{1}{i\hbar}[H_I, \boldsymbol{\rho}] - \boldsymbol{\Gamma}\boldsymbol{\rho}, \tag{14}$$

where ρ_{mn} is the density matrix element and can be expanded using the series expansion $\rho_{mn} = \rho_{mn}^{(0)} + \rho_{mn}^{(1)} + \cdots + \rho_{mn}^{(r)} + \cdots$, H_I represents the corresponding interaction Hamiltonian, and $\boldsymbol{\Gamma}$ is the transverse relaxation rate; we can obtain the equation of motion of each order density matrix element.

The derivative process of three output signals $\mathbf{E}_{S1}$, $\mathbf{E}_{S2}$, and $\mathbf{E}_{S3}$ in the three-mode system can be described by the perturbation chains:

$$\text{PA-FWM1} : \rho_{11}^{(0)} \xrightarrow{\omega_1} \rho_{31}^{(1)} \xrightarrow{\omega_{S1}} \rho_{21}^{(2)} \xrightarrow{\omega_1} \rho_{31(S2)}^{(3)},$$

$$\text{PA-FWM1} : \rho_{22}^{(0)} \xrightarrow{\omega_1} \rho_{32}^{(1)} \xrightarrow{\omega_2} \rho_{12}^{(2)} \xrightarrow{\omega_1} \rho_{32(S1)}^{(3)},$$

$$\text{PA-FWM2} : \rho_{11}^{(0)} \xrightarrow{\omega_3} \rho_{31}^{(1)} \xrightarrow{\omega_{S3}} \rho_{21}^{(2)} \xrightarrow{\omega_1} \rho'^{(3)}_{31(S2)},$$

$$\text{PA-FWM2} : \rho_{22}^{(0)} \xrightarrow{\omega_1} \rho_{32}^{(1)} \xrightarrow{\omega_2} \rho_{12}^{(2)} \xrightarrow{\omega_3} \rho_{32(S3)}^{(3)}.$$

The first step $\rho_{11}^{(0)} \xrightarrow{\omega_1} \rho_{31}^{(1)}$ expresses that an atom in the ground state $\rho_{11}^{(0)}$ absorbs a pump photon ω_1 and transitions to the excited state $\rho_{31}^{(1)}$. The second and third steps can be understood similarly. Assume that the atoms are at energy level $|1\rangle$ initially; therefore, the initial conditions are $\rho_{11}^{(0)} = 1$, and other zero-order density matrix elements are all zero. Under the steady-state approximation and the weak field approximation (i.e., the amplitude of the signal field is far less than the pump field), the third-order density matrix element can be solved according to the perturbation chains as follows:

$$\text{PA-FWM1} : \rho_{31(S2)}^{(3)} = -\frac{i\Omega_1^2\Omega_{S1}}{d_{31}d_{21}d'_{31}}, \tag{15a}$$

$$\text{PA-FWM1} : \rho_{32(S1)}^{(3)} = -\frac{i\Omega_1^2\Omega_2}{d_{32}d_{12}d'_{32}}, \tag{15b}$$

$$\text{PA-FWM2} : \rho'^{(3)}_{31(S2)} = -\frac{i\Omega_1\Omega_3\Omega_{S3}}{d''_{31}d'_{21}d'''_{31}}, \tag{15c}$$

$$\text{PA-FWM2} : \rho_{32(S3)}^{(3)} = -\frac{i\Omega_1\Omega_2\Omega_3}{d_{32}d'_{12}d''_{32}}, \tag{15d}$$

where $\Omega_i = \mu E_i/\hbar$ is the Rabi frequency of field $\mathbf{E}_i$. Here, $d_{31} = \Gamma_{31} + i\Delta_1$, $d_{21} = \Gamma_{21} + i(\Delta_1 - \Delta_{S1})$, $d'_{31} = \Gamma_{31} + i(\Delta_1 - \Delta_{S1} + \Delta'_1)$, $d_{32} = \Gamma_{32} + i\Delta'_1$, $d_{12} = \Gamma_{12} + i(\Delta'_1 - \Delta_{S2})$, $d'_{32} = \Gamma_{32} + i(\Delta'_1 - \Delta_{S2} + \Delta_1)$, $d''_{31} = \Gamma_{31} + i\Delta_3$, $d'_{21} = \Gamma_{21} + i(\Delta_3 - \Delta_{S3})$, $d'''_{31} = \Gamma_{31} + i(\Delta_3 - \Delta_{S3} + \Delta'_1)$, $d'_{12} = \Gamma_{12} + i(\Delta'_1 - \Delta'_{S2})$, and $d''_{32} = \Gamma_{32} + i(\Delta'_1 - \Delta'_{S2} + \Delta_3)$. Also, Δ_{S1}, Δ_{S2}, and Δ_{S3} represent the frequency detuning of the signals $\mathbf{E}_{S1}$, $\mathbf{E}_{S2}$, and $\mathbf{E}_{S3}$. Furthermore, Δ_1 and Δ'_1 are the frequency detuning of the fields $\mathbf{E}_1$ from the transitions $|1\rangle \rightarrow |3\rangle$ and $|2\rangle \rightarrow |3\rangle$, respectively, defined as the difference between the resonant transition frequency and laser frequency, and Δ_3 is the frequency detuning of the fields $\mathbf{E}_3$.

Due to the frequencies ω_{Si} of generated photons with small quantum deviations δ_i around the corresponding central

TABLE I. Resonance frequencies of the coherent channels in the three-mode DELC-FWM processes.

Coherence channels	Resonance frequencies of the coherent channels			
	δ_1	δ_2	δ_2'	δ_3
C1	$\delta_1 = -\Delta_1'$	$\delta_2 = \Delta_1'$	$\delta_2' = \Delta_1'$	$\delta_3 = -\Delta_1'$
C2	$\delta_1 = \frac{\Delta_1+\sqrt{\Delta_1^2+4\Gamma_{21}\Gamma_{23}+4\Omega_1^2}}{2}$	$\delta_2 = -\frac{\Delta_1+\sqrt{\Delta_1^2+4\Gamma_{21}\Gamma_{23}+4\Omega_1^2}}{2}$	$\delta_2' = -\frac{\Delta_1+\sqrt{\Delta_1^2+4\Gamma_{21}\Gamma_{23}+4\Omega_1^2}}{2}$	$\delta_3 = \frac{\Delta_1+\sqrt{\Delta_1^2+4\Gamma_{21}\Gamma_{23}+4\Omega_1^2}}{2}$
C3	$\delta_1 = \frac{\Delta_1-\sqrt{\Delta_1^2+4\Gamma_{21}\Gamma_{23}+4\Omega_1^2}}{2}$	$\delta_2 = -\frac{\Delta_1-\sqrt{\Delta_1^2+4\Gamma_{21}\Gamma_{23}+4\Omega_1^2}}{2}$	$\delta_2' = -\frac{\Delta_1-\sqrt{\Delta_1^2+4\Gamma_{21}\Gamma_{23}+4\Omega_1^2}}{2}$	$\delta_3 = \frac{\Delta_1-\sqrt{\Delta_1^2+4\Gamma_{21}\Gamma_{23}+4\Omega_1^2}}{2}$

frequency ϖ_{Si}, ω_{Si} can be written as $\omega_{Si} = \varpi_{Si} + \delta_i$ ($i = 1$, 2, 3) with the limitation of $|\delta_i| \ll \varpi_{Si}$. Considering quantum deviation δ_1, the frequency detuning of the signals $\mathbf{E}_{S1}$ can be expressed as $\Delta_{S1} = \omega_{32} - \omega_{S1} = \omega_{32} - (\varpi_S 1 + \delta_1) = \Delta_1 - \delta_1$. According to the conservation of energy in PA-FWM1 and PA-FWM2, $\delta_2 = -\delta_1$ and $\delta_3 = \delta_1$, which show the frequency correlation of the triphoton state in this three-mode energy-level-cascaded system. Different quantum properties of the triphoton state can also be reflected by focusing on these photon deviations. In the resonance conditions of coupling fields, the third-order density matrix element $\rho_{31(S2)}^{(3)}$ in Eq. (12b) with the expression of Δ_{S1} can be rewritten as follows:

$$\rho_{31(S2)}^{(3)} = \frac{-i\Omega_1^2\Omega_{S1}}{(\Gamma_{31} + i\Delta_1)(\Gamma_{21} + i\delta_1)(\Gamma_{31} + i\delta_1 + i\Delta'_1)}. \quad (16)$$

The third-order density matrix element $\rho^{(3)}$ is proportional to the third-order nonlinear susceptibility $\chi^{(3)}$, which determines the strength of the nonlinear interaction and therefore affects the gain of the nonlinear process according to Eqs. (8a)–(8c). Using atomic coherence, parametric gain properties of this quantum interplay can be directly adjusted by modulating the dressing effect. A laser field, especially from the same laser as pump field $\mathbf{E}_1$, is added as a dressing field to modulate the energy levels involved in the PA-FWM process. When we consider the dressing effect of $\mathbf{E}_1$, the perturbation chain of $\mathbf{E}_{S2}$ can be expressed as

$$\rho_{11}^{(0)} \xrightarrow{\omega_1} \rho_{31}^{(1)} \xrightarrow{\omega_{S1}} \rho_{2\Omega_1\pm}^{(2)} \xrightarrow{\omega_1} \rho_{31(S2)D}^{(3)}.$$

The subscript 1 of $\rho_{21}^{(2)}$ is replaced by $\Omega_1\pm$, which indicates that dressing fields $\mathbf{E}_1$ dress the level $|1\rangle$ and influence the identical coherence between states $|1\rangle$ and $|3\rangle$. The third-order density matrix element in Eq. (16) with a single dress can be rewritten as follows:

$$\rho_{31(S2)D}^{(3)} = \frac{-i\Omega_1^2\Omega_{S1}}{\left[(\Gamma_{31} + i\Delta_1)\left(\Gamma_{21} + i\delta_1 + \frac{\Omega_1^2}{\Gamma_{23}+i\delta_1-i\Delta_1}\right)\right](\Gamma_{31} + i\delta_1 + i\Delta'_1)}. \quad (17)$$

By maximizing the denominator of the third-order density matrix element, we can obtain the resonance positions as shown in Table I. Figure 9 shows the third-order density matrix element in the perturbation chains under different conditions and exhibits the resonance positions of small quantum deviations window δ_i, which is the frequency corresponding to the coherent channels. The first and second rows are the Stokes and anti-Stokes signals of PA-FWM1, respectively. The third and fourth rows are the Stokes and anti-Stokes signals of PA-FWM2, respectively. A set of longitudinal resonance positions corresponds to one coherent channel and a single FWM mode. The dressing field $\mathbf{E}_1$ creates the dressed states $|1\pm\rangle$ from $|1\rangle$, as shown in Fig. 10. It results in two coexisting PA-FWM coherent channels, and the output signals thus have two modes of different frequencies, and therefore, the number of coherent channels are increased. In Fig. 9, with the dressing effect, peak (II) split into two peaks (IV) and (V) denoted by the dressing term in Eq. (16). Three coherent channels coexist (IV, V, and VI), all satisfying the energy conservation condition $\delta_1 + \delta_2 + \delta_2' + \delta_3 = 0$. The quantum information capacity, expressed as n^3, where n represents the number of coherent channels, is greatly expanded to 3^3 in this single dressing system.

Subsequently, the Duan and PPT criteria in each coherent channel are investigated in the three- and four-mode DELC-FWM system. According to Eq. (16), we can obtain the dressing-modulated optical gain, and then the entanglement characteristics can be actively and directly controlled in the process of preparing the entangled sources. Figure 11 shows the values of criteria vs δ_1, where the gain of the first PA-FWM is modulated by the dressing field $\mathbf{E}_1$. Here, we set $G_2 = 1.2$ in the three-mode system and $G_2 = 1.3$ and $G_3 = 1.1$ in the four-mode system. The red areas, where the Duan are not violated or the PPT values are not negative, indicate the absence of entanglement. The unentangled modes are not given in this figure, including $\hat{a}_1 - \hat{a}_3$ in the three mode and $\hat{a}_1 - \hat{a}_3$, $\hat{a}_2 - \hat{a}_4$, $\hat{a}_3 - \hat{a}_4$, $\hat{a}_3 - \{\hat{a}_1\hat{a}_4\}$, and $\hat{a}_4 - \{\hat{a}_2\hat{a}_3\}$ in four mode. The black dashed areas correspond to the coherent channels, where the gains are stronger. Also, the gains in channels are independent and do not interfere with each other, so the values of the criteria are different.

V. DISCUSSION AND CONCLUSIONS

In addition to the case of the second-order density matrix element $\rho_{21}^{(2)}$ dressed by the field $\mathbf{E}_1$ mentioned above, it can also be expanded to many other dressing cases. The first-order density matrix element $\rho_{31}^{(1)}$ under the condition of the energy level $|1\rangle$ dressed by the field $\mathbf{E}_1$ can be written as Eq. (18), which is obtained by the perturbation chain: $\rho_{11}^{(0)} \xrightarrow{\omega_1} \rho_{3\Omega_1\pm}^{(1)} \xrightarrow{\omega_{S1}} \rho_{21}^{(2)} \xrightarrow{\omega_1} \rho_{31(S2)D}^{(3)}$.

$$\rho_{31(S2)D}^{(3)} = \frac{-i\Omega_1^2\Omega_{S1}}{\left(\Gamma_{31} + i\Delta_1 + \frac{\Omega_1^2}{\Gamma_{33}}\right)(\Gamma_{21} + i\delta_1)(\Gamma_{31} + i\delta_1 + i\Delta'_1)}. \quad (18)$$

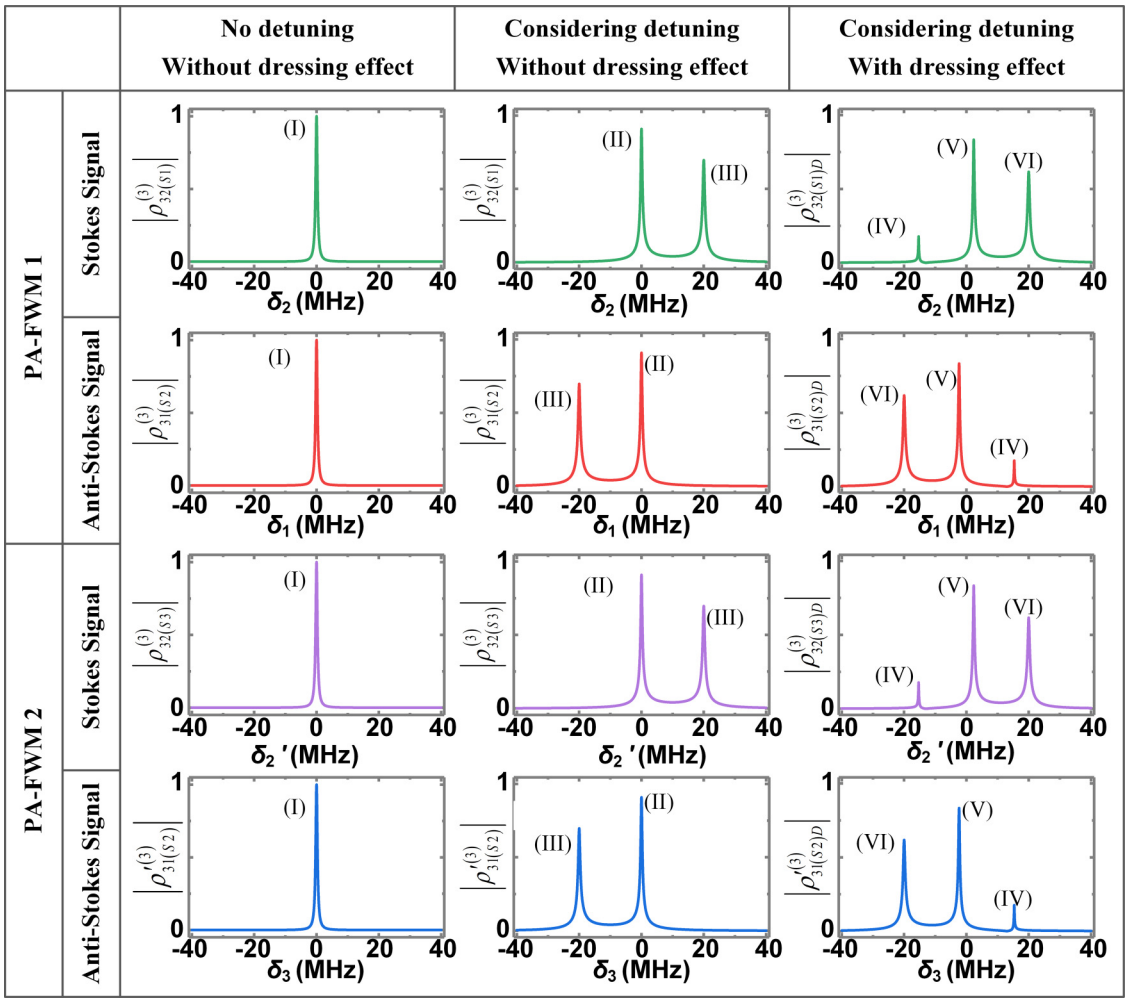

FIG. 9. Theoretically calculated normalized third-order density matrix where the dressing effect acts on the second-order density matrix element $\rho_{21}^{(2)}$. The conditions of three columns are different. The conditions of the first column are $\Delta_1 = \Delta_1^{'} = 0$, without the dressing effect. The conditions of the second column are $\Delta_1 = 13$ MHz and $\Delta_1^{'} = 20$ MHz, without the dressing effect. The conditions of the third column are $\Delta_1 = 13$ MHz and $\Delta_1^{'} = 20$ MHz, with the dressing effect of field $\mathbf{E}_1$.

The resonance positions of the coherent channels are $\delta_1 = 0$ and $\delta_1 = -\Delta_1'$. The number of coherent channels is still 2, and the resonance peaks are not split by the dressing effect, which is shown in Fig. 12. The third-order density matrix element $\rho_{31}^{(3)}$ dressed by the field $\mathbf{E}_1$ at energy level $|1\rangle$ can be written as Eq. (19), which is obtained by the perturbation chain: $\rho_{11}^{(0)} \xrightarrow{\omega_1} \rho_{31}^{(1)} \xrightarrow{\omega_{S1}} \rho_{21}^{(2)} \xrightarrow{\omega_1} \rho_{3\Omega_1\pm(S2)D}^{(3)}$.

$$\rho_{31(S2)D}^{(3)} = \frac{-i\Omega_1^2\Omega_{S1}}{\left[(\Gamma_{31}+i\Delta_1)(\Gamma_{21}+i\delta_1)\left(\Gamma_{31}+i\delta_1+i\Delta'_1+\frac{\Omega_1^2}{\Gamma_{33}+i\delta_1+i\Delta'_1-i\Delta_1}\right)\right]}. \tag{19}$$

The resonance positions of the three coherent channels are $\delta_1 = 0$, $\delta_1 = (\Delta_1 - 2\Delta'_1 + \sqrt{\Delta})/2$, and $\delta_1 = (\Delta_1 - 2\Delta'_1 - \sqrt{\Delta})/2$, where $\Delta = (\Delta_1 - 2\Delta'_1)^2 - 4(\Delta'^2_1 - \Delta_1\Delta'_1 - \Omega_1^2 - \Gamma_{31}\Gamma_{33})$, which is like Fig. 9, but the frequency difference of the latter two peaks is $\sqrt{\Delta}$. The phenomenon of split resonance peaks observed in the experiment is generally caused by the dressed second-order density matrix element $\rho^{(2)}$ because the detuning of deriving $\rho^{(2)}$ is smaller, with stronger dressing effect, than deriving $\rho^{(3)}$.

Moreover, the pump field $\mathbf{E}_3$ can also be used as a dressing field. The second-order density matrix element $\rho_{21}^{(2)}$ dressed by the field $\mathbf{E}_3$ at energy level $|1\rangle$ can be written as Eq. (20), which is obtained by the perturbation chain: $\rho_{11}^{(0)} \xrightarrow{\omega_1} \rho_{31}^{(1)} \xrightarrow{\omega_{S1}} \rho_{2\Omega_3\pm}^{(2)} \xrightarrow{\omega_1} \rho_{31(S2)D}^{(3)}$.

$$\rho_{31(S2)D}^{(3)} = \frac{-i\Omega_1^2\Omega_{S1}}{\left[(\Gamma_{31}+i\Delta_1)\left(\Gamma_{21}+i\delta_1+\frac{\Omega_3^2}{\Gamma_{23}+i\delta_1-i\Delta_3}\right)(\Gamma_{31}+i\delta_1+i\Delta'_1)\right]}. \tag{20}$$

Here, the resonance positions and the optical gains of the coherent channels depends on the Rabi frequency Ω_3 and frequency detuning Δ_3 of the dressing field $\mathbf{E}_3$. The three coherent channels are at $\delta_1 = (\Delta_3 + \sqrt{\Delta_3^2 + 4\Gamma_{21}\Gamma_{23} + 4\Omega_3^2})/2$, $\delta_1 = (\Delta_3 - \sqrt{\Delta_3^2 + 4\Gamma_{21}\Gamma_{23} + 4\Omega_3^2})/2$, and $\delta_1 = -\Delta_1'$.

In summary, the DELC-FWM processes are proposed to produce the three- and four-mode quantum entangled states in Rb atomic vapors in one step. We apply the Duan and

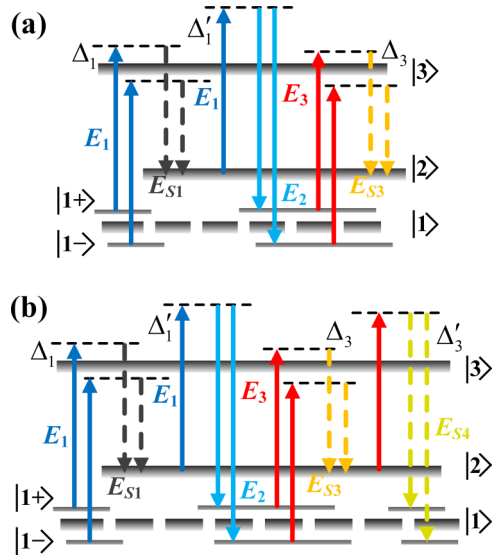

FIG. 10. The energy-level diagram in the dressed-state picture. (a) Three-mode system. (b) Four-mode system. The energy levels $|1\pm\rangle$ are created from $|1\rangle$. Multiple coherent channels of four-wave mixing (FWM) are constructed because of the strong dressing effect of the field $\mathbf{E}_1$.

PPT criteria to characterize the multipartite entanglement potentially existing in this cascaded system and theoretically investigate the dependence of criteria on the system parameters. Furthermore, the dressing field is introduced to produce and coherently control the multimode multiplexed entanglement via constructing multiple coherent channels of FWM. The properties of the entanglement among output beams are coherent-channel dependent and can be well controlled using the dressing effect of atoms and many optical parameters in our system, without need of extra control (e.g., beam splitters) after the quantum interplay. In our scheme, using atomic coherence, the generation and modulation of multipartite entanglement can be integrated in the process of the entangled states preparation. These results may be helpful for multimode quantum secure communication, quantum routing, and quantum coherent control.

ACKNOWLEDGMENTS

This paper was supported by the National Key R&D Program of China (Grants No. 2017YFA0303700 and No. 2018YFA0307500), National Natural Science Foundation of China (Grants No. 61975159, No. 11904279, No. 12174302, No. 62022066, No. 12074306, and No. 12074303), and Key Scientific and Technological Innovation Team of Shaanxi Province (Grant No. 2021TD-56).

APPENDIX

The three- and four-mode DELC-FWM systems correspond to cascade Rb cells in terms of obtaining multiple entangled states, as shown in Figs. 2 and 4. As DELC-FWM only requires a single Rb cell, it introduces fewer vacuum losses. Moreover, this method is phase insensitive without the need for a complicated phase-locking technique.

Figure 12 shows the resonance positions of the small quantum deviations window δ_i under the condition of the dressed first-order density matrix element $\rho^{(1)}$ [Eq. (18)]. Since the process of deriving $\rho^{(1)}$ is independent of the quantum deviation, the resonance peak does not split because of the dressing effect acting on $\rho^{(1)}$.

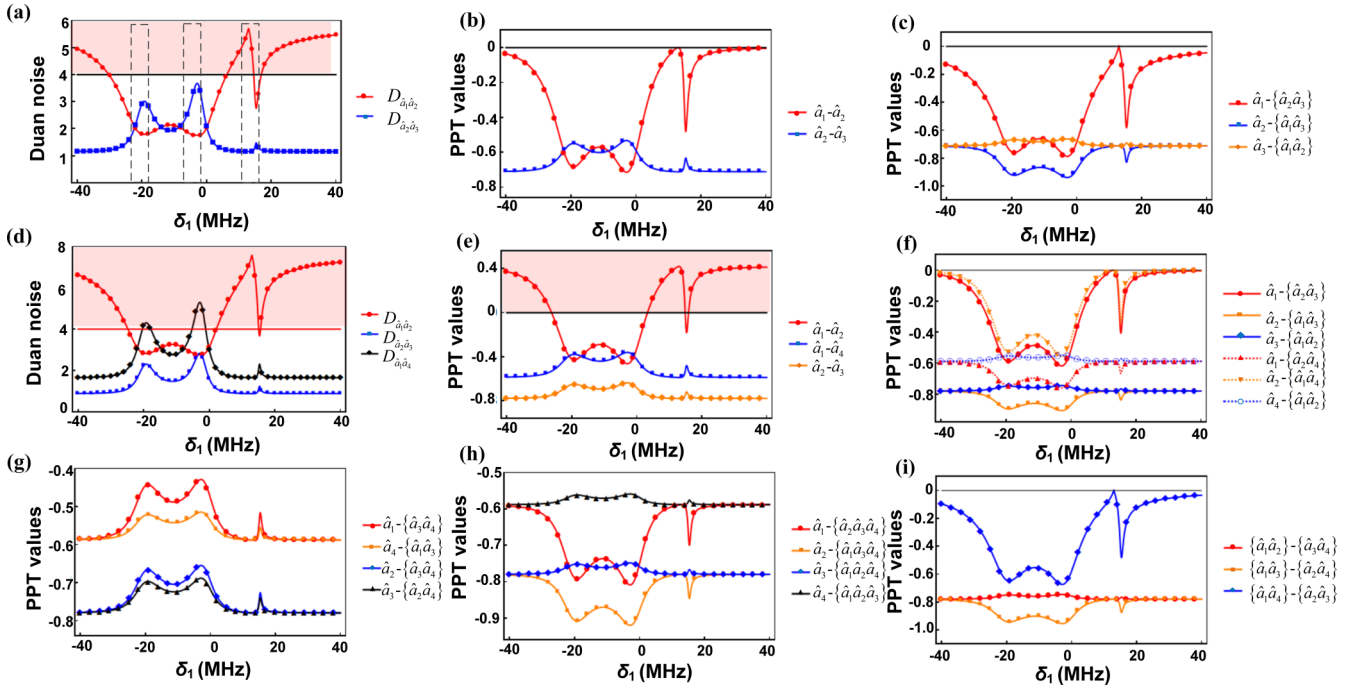

FIG. 11. Entanglement criteria in three coherent channels with single dressing effect. (a) Three-mode Duan criterion. (b) and (c) Three-mode positivity under partial transposition (PPT) criterion. (d) Four-mode Duan criterion. (e)–(i) Four-mode PPT criterion. The red areas indicate no entanglement. The black dashed areas show the criterion in each channel.

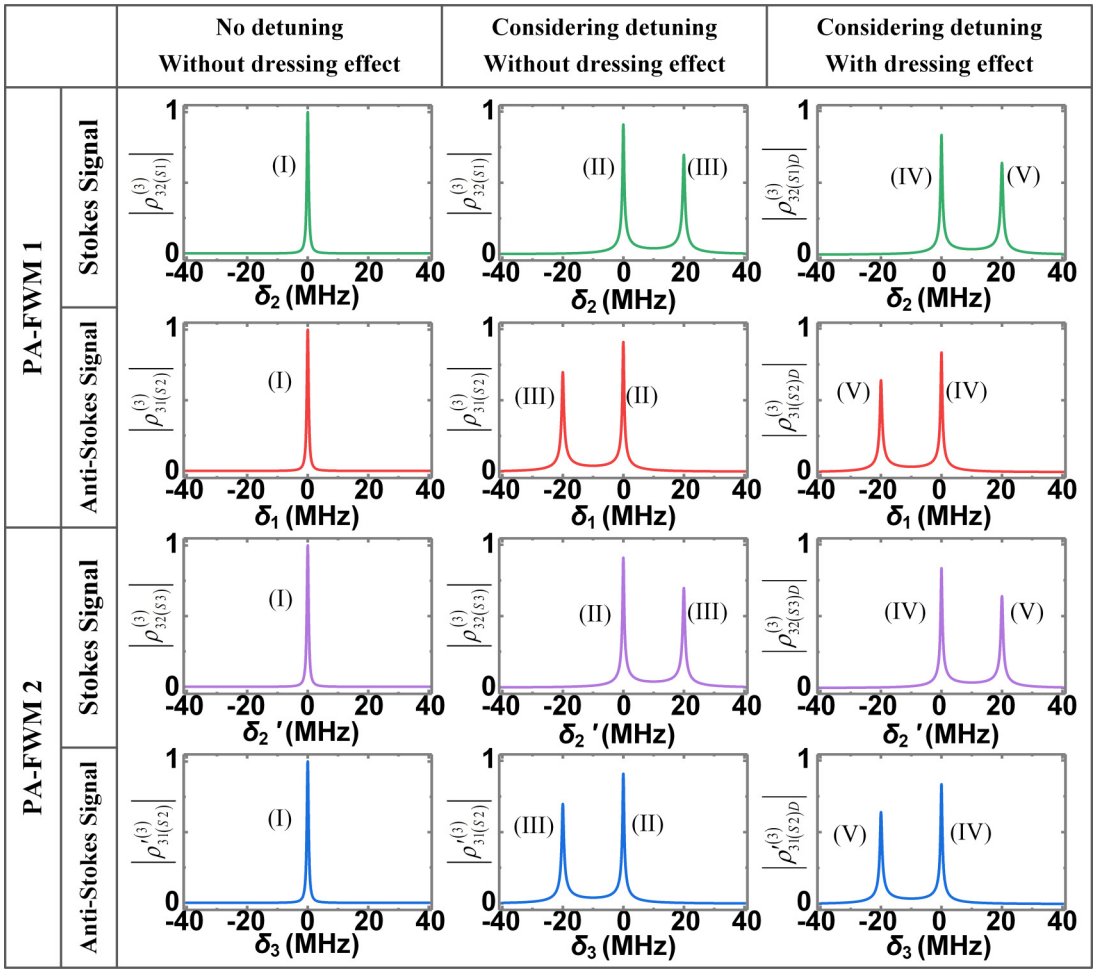

FIG. 12. Theoretically calculated normalized third-order density matrix element where the dressing effect acts on the first-order density matrix element $\rho_{31}^{(1)}$. The conditions of three columns are different. The conditions of the first column are $\Delta_1 = \Delta_1^{'} = 0$, without the dressing effect. The conditions of the second column are $\Delta_1 = 13\,\mathrm{MHz}$ and $\Delta_1^{'} = 20$ MHz, without the dressing effect. The conditions of the third column are $\Delta_1 = 13\,\mathrm{MHz}$ and $\Delta_1^{'} = 20$ MHz, with the dressing effect of field $\mathbf{E}_1$.

[1] V. Giovannetti, S. Lloyd, and L. Maccone, Quantum Metrology, Phys. Rev. Lett. **96**, 010401 (2006).

[2] R. Horodecki, P. Horodecki, M. Horodecki, and K. Horodecki, Quantum entanglement, Rev. Mod. Phys. **81**, 865 (2009).

[3] C. Weedbrook, S. Pirandola, R. García-Patrón, N. J. Cerf, T. C. Ralph, J. H. Shapiro, and S. Lloyd, Gaussian quantum information, Rev. Mod. Phys. **84**, 621 (2012).

[4] J. W. Pan, Z. B. Chen, C. Y. Lu, H. Weinfurter, A. Zeilinger, and M. Zukowski, Multiphoton entanglement and interferometry, Rev. Mod. Phys. **84**, 777 (2012).

[5] C. Fabre and N. Treps, Modes and states in quantum optics, Rev. Mod. Phys. **92**, 035005 (2020).

[6] P. G. Kwiat, K. Mattle, H. Weinfurter, A. Zeilinger, A. V. Sergienko, and Y. Shih, New High-Intensity Source of Polarization-Entangled Photon Pairs, Phys. Rev. Lett. **75**, 4337 (1995).

[7] A. G. White, D. F. V. James, P. H. Eberhard, and P. G. Kwiat, Nonmaximally Entangled States: Production, Characterization, and Utilization, Phys. Rev. Lett. **83**, 3103 (1999).

[8] J. Pan, D. Bouwmeester, M. Daniell, H. Weinfurter, and A. Zeilinger, Experimental test of quantum nonlocality in three-photon Greenberger-Horne-Zeilinger entanglement, Nature (London) **403**, 515 (2000).

[9] Y. Huang, B. Liu, L. Peng, Y. Li, L L., C. Li, and G. Guo, Experimental generation of an eight-photon Greenberger-Horne-Zeilinger state, Nat. Commun. **2**, 546 (2011).

[10] X. Yao, T. Wang, P. Xu, H. Lu, G. Pan, X. Bao, C. Peng, C. Lu, Y. Chen, and J. Pan, Observation of eight-photon entanglement, Nature Photon. **6**, 225 (2012).

[11] L. A. Wu, H. J. Kimble, J. L. Hall, and H. Wu, Generation of Squeezed States by Parametric Down Conversion, Phys. Rev. Lett. **57**, 2520 (1986).

[12] A. Heidmann, R. J. Horowicz, S. Reynaud, E. Giacobino, C. Fabre, and G. Camy, Observation of Quantum Noise Reduction on Twin Laser Beams, Phys. Rev. Lett. **59**, 2555 (1987).

[13] K. S. Zhang, T. Coudreau, M. Martinelli, A. Maître, and C. Fabre, Generation of bright squeezed light at 1.06 μm using cascaded nonlinearities in a triply resonant cw

periodically-poled lithium niobate optical parametric oscillator, Phys. Rev. A **64**, 033815 (2001).

[14] X. L. Su, A. H. Tan, X. J. Jia, J. Zhang, C. D. Xie, and K. C. Peng, Experimental Preparation of Quadripartite Cluster and Greenberger-Horne-Zeilinger Entangled States for Continuous Variables, Phys. Rev. Lett. **98**, 070502 (2007).

[15] M. Yukawa, R. Ukai, P. van Loock, and A. Furusawa, Experimental generation of four-mode continuous-variable cluster states, Phys. Rev. A **78**, 012301 (2008).

[16] A. S. Coelho, F. A. S. Barbosa, K. N. Cassemiro, A. S. Villar, M. Martinelli, and P. Nussenzveig, Three-color entanglement, Science **326**, 823 (2009).

[17] X. Jia, Z. Yan, Z. Duan, X. Su, H. Wang, C. Xie, and K. Peng, Experimental Realization of Three-Color Entanglement at Optical Fiber Communication and Atomic Storage Wavelengths, Phys. Rev. Lett. **109**, 253604 (2012).

[18] M. Chen, N. C. Menicucci, and O. Pfister, Experimental Realization of Multipartite Entanglement of 60 Modes of a Quantum Optical Frequency Comb, Phys. Rev. Lett. **112**, 120505 (2014).

[19] Y. Cai, J. Roslund, G. Ferrini, F. Arzani, X. Xu, C. Fabre, and N. Treps, Multimode entanglement in reconfigurable graph states using optical frequency combs, Nat. Commun. **8**, 15645 (2017).

[20] S. Armstrong, J. F. Morizur, J. Janousek, B. Hage, N. Treps, P. K. Lam, and H. A. Bachor, Programmable multimode quantum networks, Nat. Commun. **3**, 1026 (2012).

[21] M. V. Larsen, X. Guo, C. R. Breum, J. S. Neergaard-Nielsen, and U. L. Andersen, Deterministic generation of a two-dimensional cluster state, Science **366**, 369 (2019).

[22] W. Asavanant, Y. Shiozawa, S. Yokoyama, B. Charoensombutamon, H. Emura, R. N. Alexander, S. Takeda, J. Yoshikawa, N. C. Menicucci, H. Yonezawa *et al.*, Generation of time-domain-multiplexed two-dimensional cluster state, Science **366**, 373 (2019).

[23] N. Treps, N. Grosse, W. P. Bowen, C. Fabre, H. A. Bachor, and P. K. Lam, A quantum laser pointer, Science **301**, 940 (2003).

[24] X. Guo, C. R. Breum, J. Borregaard, S. Izumi, and U. L. Andersen, Distributed quantum sensing in a continuous-variable entangled network, Nature Phys. **16**, 281 (2020).

[25] Y. Cai, J. Roslund, V. Thiel, C. Fabre, and N. Treps, Quantum enhanced measurement of an optical frequency comb, Npj Quantum Inf. **7**, 82 (2021).

[26] R. Ukai, N. Iwata, Y. Shimokawa, S. C. Armstrong, A. Politi, J. I. Yoshikawa, P. van Loock, and A. Furusawa, Demonstration of Unconditional One-Way Quantum Computations for Continuous Variables, Phys. Rev. Lett. **106**, 240504 (2011).

[27] X. Su, S. Hao, X. Deng, L. Ma, M. Wang, X. Jia, C. Xie, and K. Peng, Gate sequence for continuous variable one-way quantum computation, Nat. Commun. **4**, 2828 (2013).

[28] M. V. Larsen, X. Guo, C. R. Breum, J. S. Neergaard-Nielsen, and U. L. Andersen, Deterministic multi-mode gates on a scalable photonic quantum computing platform, Nat. Phys. **17**, 1018 (2021).

[29] S. Armstrong, M. Wang, R. Y. Teh, Q. Gong, Q. He, J. Janousek, H. A. Bachor, M. D. Reid, and P. K. Lam, Multipartite Einstein-Podolsky-Rosen steering and genuine tripartite entanglement with optical networks, Nat. Phys. **11**, 167 (2015).

[30] C. F. McCormick, V. Boyer, E. Arimondo, and P. D. Lett, Strong relative intensity squeezing by four-wave mixing in rubidium vapor, Opt. Lett. **32**, 178 (2007).

[31] C. F. McCormick, A. M. Marino, V. Boyer, and P. D. Lett, Strong low-frequency quantum correlations from a four-wave-mixing amplifier, Phys. Rev. A **78**, 043816 (2008).

[32] V. Boyer, A. M. Marino, R. C. Pooser, and P. D. Lett, Entangled images from four-wave mixing, Science **321**, 544 (2008).

[33] C. Liu, J. Jing, Z. Zhou, R. C. Pooser, F. Hudelist, L. Zhou, and W. Zhang, Realization of low frequency and controllable bandwidth squeezing based on a four-wave-mixing amplifier in rubidium vapor, Opt. Lett. **36**, 2979 (2011).

[34] V. Boyer, A. M. Marino, and P. D. Lett, Generation of Spatially Broadband Twin Beams for Quantum Imaging, Phys. Rev. Lett. **100**, 143601 (2008).

[35] C. S. Embrey, M. T. Turnbull, P. G. Petrov, and V. Boyer, Observation of Localized Multi-Spatial-Mode Quadrature Squeezing, Phys. Rev. X **5**, 031004 (2015).

[36] Y. Cai, L. Hao, D. Zhang, Y. Liu, B. Luo, Z. Zheng, F. Li, and Y. Zhang, Multimode entanglement generation with dual-pumped four-wave-mixing of rubidium atoms, Opt. Express **28**, 25278 (2020).

[37] K. Zhang, W. Wang, S. Liu, X. Pan, J. Du, Y. Lou, S. Yu, S. Lv, N. Treps, C. Fabre, and J. Jing, Reconfigurable Hexapartite Entanglement by Spatially Multiplexed Four-Wave Mixing Processes, Phys. Rev. Lett. **124**, 090501 (2020).

[38] Z. Qin, L. Cao, H. Wang, A. M. Marino, W. Zhang, and J. Jing, Experimental Generation of Multiple Quantum Correlated Beams from Hot Rubidium Vapor, Phys. Rev. Lett. **113**, 023602 (2014).

[39] Y. Cai, J. Feng, H. Wang, G. Ferrini, X. Xu, J. Jing, and N. Treps, Quantum-network generation based on four-wave mixing, Phys. Rev. A **91**, 013843 (2015).

[40] A. M. Marino, R. C. Pooser, V. Boyer, and P. D. Lett, Tunable delay of Einstein-Podolsky-Rosen entanglement, Nature (London) **457**, 859 (2009).

[41] S. Li, X. Pan, Y. Ren, H. Liu, S. Yu, and J. Jing, Deterministic Generation of Orbital-Angular-Momentum Multiplexed Tripartite Entanglement, Phys. Rev. Lett. **124**, 083605 (2020).

[42] Y. Zhang, A. W. Brown, and M. Xiao, Opening Four-Wave Mixing and Six-Wave Mixing Channels Via Dual Electromagnetically Induced Transparency, Phys. Rev. Lett. **99**, 123603 (2007).

[43] H. Yan, S. Zhang, J. F. Chen, M. M. T. Loy, G. K. L. Wong, and S. Du, Generation of Narrow-Band Hyperentangled Nondegenerate Paired Photons, Phys. Rev. Lett. **106**, 033601 (2011).

[44] Y. Mei, Y. Zhou, S. Zhang, J. Li, K. Liao, H. Yan, S. L. Zhu, and S. Du, Einstein-Podolsky-Rosen Energy-Time Entanglement of Narrow-Band Biphotons, Phys. Rev. Lett. **124**, 010509 (2020).

[45] D. Zhang, C. Li, Z. Zhang, Y. Zhang, Y. Zhang, and M. Xiao, Enhanced intensity-difference squeezing via energy-level modulations in hot atomic media, Phys. Rev. A **96**, 043847 (2017).

[46] C. Li, B. Gu, D. Zhang, W. Chen, Z. Shen, G. Lan, and Y. Zhang, Modulation gain and squeezing by dressed state in hot atomic system, Laser Phys. Lett. **16**, 055401 (2019).

[47] Y. Liu, K. Li, W. Li, S. Li, Y. Cai, and Y. Zhang, Dressing-controlled quantum steering in energy-level cascaded

parametric amplified four-wave mixing process, Adv. Quantum Tecnol. **3**, 2000029 (2020).

[48] L. M. Duan, G. Giedke, J. I. Cirac, and P. Zoller, Inseparability Criterion for Continuous Variable Systems, Phys. Rev. Lett. **84**, 2722 (2000).

[49] R. Simon, Peres-Horodecki Separability Criterion for Continuous Variable Systems, Phys. Rev. Lett. **84**, 2726 (2000).

[50] R. F. Werner and M. M. Wolf, Bound Entangled Gaussian States, Phys. Rev. Lett. **86**, 3658 (2001).

[51] M. D. Reid and D. F. Walls, Quantum theory of nondegenerate four-wave mixing, Phys. Rev. A. **34**, 4929 (1986).

[52] J. Li, W. Li, M. Niu, Y. Lin, C. Li, Y. Cai, and Y. Zhang, Generation of multimode quantum correlation with energy-level cascaded four-wave mixing processes, Ann. Phys. **422**, 168316 (2020).